Research Article

Xuefang Wang*, Xianshan Dong, Junfeng Xiao, YuYu Zhang, Jianfeng Xu, Sheng Liu, and Liang Gao

Quantum effects of gas flow in nanochannels

https://doi.org/10.1515/ntrev-2021-0022
received March 10, 2021; accepted March 29, 2021

Abstract: Based on the thermal theory of Newtonian mechanics, the pressure difference in the macro channels will drive the gas flow until the pressure difference inside is zero. However, the 12-year vacuum packaging experiments in our laboratory showed that when the macroscopic channel is reduced to a critical size and reaches the nanometer level, the gas flow inside the channel is hindered, that is, the differential pressure cannot become zero. To explain this paradoxical phenomenon, this study analyzes the flow of air molecules in the channel by using the De Broglie's matter waves and Heisenberg's uncertainty principle. Based on the law of quantum mechanics, when the diameter of the nanochannel is reduced to a certain size, it has a localized high pressure in the channel, which impedes the gas flow. This article introduces quantum mechanics into nanochannel's gas fluid dynamics for the first time, expanding the new direction of fluid mechanics.

Keywords: gas flow hindrance, nanochannels, quantum mechanics, localized high pressure

*** Corresponding author: Xuefang Wang,** School of Mechanical Science & Engineering, Huazhong University of Science & Technology, Wuhan 430074, China, e-mail: memsman@163.com
Xianshan Dong: Science and Technology on Reliability Physics and Application of Electronic Component Laboratory, China Electronic Product Reliability and Environmental Testing Research Institute, Guangzhou 510610, China
Junfeng Xiao, Jianfeng Xu, Liang Gao: The State Key Laboratory of Digital Manufacturing Equipment and Technology, School of Mechanical Science & Engineering, Huazhong University of Science & Technology, Wuhan 430074, China
YuYu Zhang: School of Mechanical Science & Engineering, Huazhong University of Science & Technology, Wuhan 430074, China
Sheng Liu: School of Mechanical Science & Engineering, Huazhong University of Science & Technology, Wuhan 430074, China; MOE Key Laboratory of Hygro Power Transients, School of Power and Mechanical Engineering, Wuhan University, Wuhan 430072, China; Institute of Technological Sciences, Wuhan University, Wuhan 430072, China

1 Introduction

According to the thermal theory of Newtonian mechanics, when the gas components on both ends of a macroscopic channel are identical, the gas flow in the macro channel is driven by the differential pressure between the two sides of the channel. The pressure difference drives the gas flow until the pressure difference between the two sides of the channel is zero. However, our lab found that after 12 years, in the tube shell packaging experiments, the tube shell still maintains a high vacuum inside, which is inconsistent with the traditional theory, according to which the tube shell vacuum cannot be maintained for as long as 12 years. The prolonged holding of the vacuum indicates the hindrance of the gas flow in the channel.

As early as 1909, Knudsen experimentally studied the resistance properties of gas flow within the micron channel and pointed out the existence of a thin gas effect within it [1]. In 2018, Scorrano *et al.* proposed a widely applicable theoretical method for quantitatively predicting the closed gas flow in the Knudsen and transition zones. The channel sizes ranged from 2.5 to 250 nm. The validity of their established volumetric gas flow model was demonstrated by experimental measurements [2–7]. In 2019, Zhang *et al.* established a nanoscale pore model using molecular dynamics theory and simulated the transition flow and slip flow of methane molecules in carbon nanopores by molecular dynamics and found that the pore walls composed of carbon atoms have an adsorption [8–13]. In 2019, Baek and Akkutlu analyzed the average free path of gas molecules in organic nanotubes using molecular simulation, Monte Carlo simulation, and molecular dynamics and found that the nanoconfinement effect significantly changed the properties of the confined fluids and that the classical gas dynamics theory overestimated the average free path of oil and gas fluids under typical reservoir conditions [14–19]. In 2020, Hong *et al.* conducted experiments on laminar and turbulent (including blocked flow) gas flow in smooth microtubes under atmospheric backpressure and variable inlet pressure conditions and investigated their local friction factors [20–26]. The theoretical methods used in the

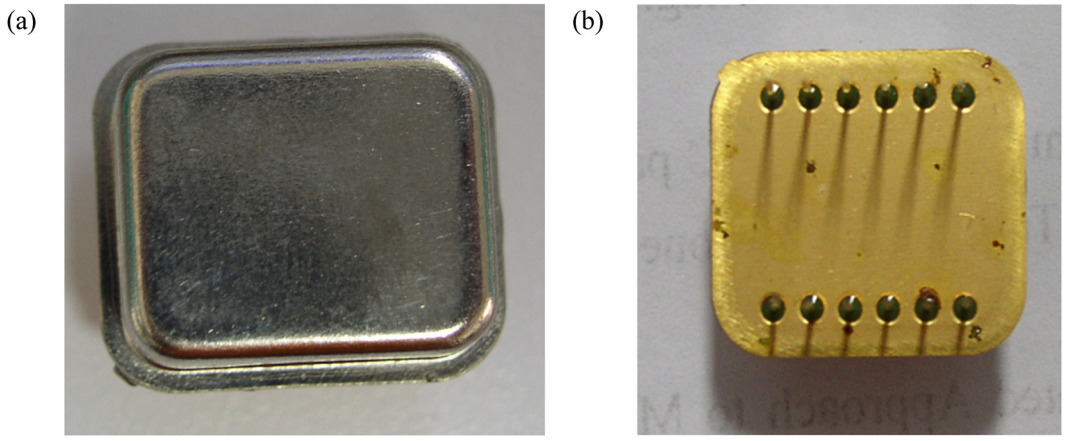

Figure 1: MD2A tube cap (a) and tube seat (b).

above studies were based on Newtonian mechanics while the scales of the investigated nanochannels were all above 2 nm and did not consider the case of channels below 1 nm. When the channel size is reduced to a certain range, the laws of the gas flow in them may no longer follow the laws of Newtonian mechanics.

In 1999, Markus Arndt demonstrated the quantum effect of a fullerene molecule (C_{60}) with 720 atomic masses [27–33]. In November 2019, the team further demonstrated the quantum effect of a short bacillus peptide molecule by double-slit interference experiments. This is a 15 amino acid length natural antibiotic with a mass of 1,882 atoms [34–40]. And the vacuum tube shells in this laboratory exhibit phenomenon that cannot yet be explained by Newtonian mechanics, namely, the maintenance of a higher vacuum for 12 years.

In this article, we consider to distinguish the gas flow in 1 nm scale nanochannels from that above 1 nm and introduce quantum mechanics to analyze the gas flow in microchannels below 1 nm scale. Whereas there are no studies to discuss the mechanism of the gas flow in the nanochannels on the scale below 1 nm, this article further introduces the De Broyne matter wave of quantum mechanics [41–46] and Heisenberg's uncertainty principle to analyze the gas flow in the nanochannels.

2 Experiment and analysis

In this study, the metal shell vacuum packaging is used as an example to analyze the nanochannels that exist inside it after vacuum packaging. As shown in Figure 1, the packaged tube shell is commonly used for hermetic packaging of electronic devices, where Figure 1(a) is the tube cap and Figure 1(b) is the tube seat. There is no getter in the tube shell, and the internal space after packaging is 2.1 cm^3.

In this study, resistance welding is used to weld the abovementioned metal tube seat and tube cap in a vacuum environment. After welding, the internal nano capillary channels are shown in Figure 2.

Based on the above experimental measurement, the vacuum packaging leakage model was established as shown in Figure 3. The external air can leak into the interior of the metal shell through the nano capillary tube. In this study, the specific leakage situation of the gas was first analyzed based on the characteristics of the airflow through the capillary pores [47,48]. The leakage rate of the gas (Q) is expressed as:

$$Q = \left[\frac{\pi d^4 \bar{p}}{128 \eta L} + \frac{1}{6} \left(\frac{2\pi RT}{M} \right)^{1/2} \frac{d^3}{L} \left(\frac{1 + \left(\frac{M}{RT} \right)^{1/2} d\bar{p}/\eta}{1 + 1.24 \left(\frac{M}{RT} \right)^{1/2} d\bar{p}/\eta} \right) \right] \times (p_1 - p_2) \quad (1)$$

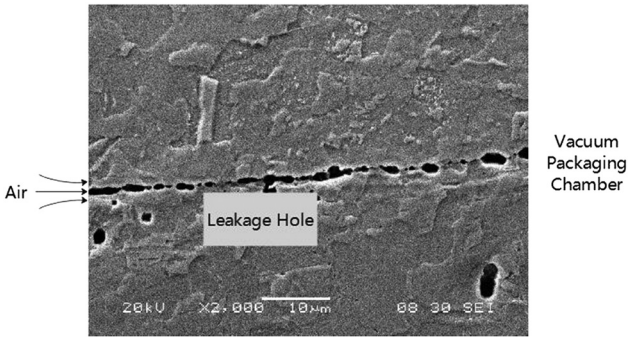

Figure 2: Cross-sectional SEM image of a typical leakage hole in a vacuum packaging shell.

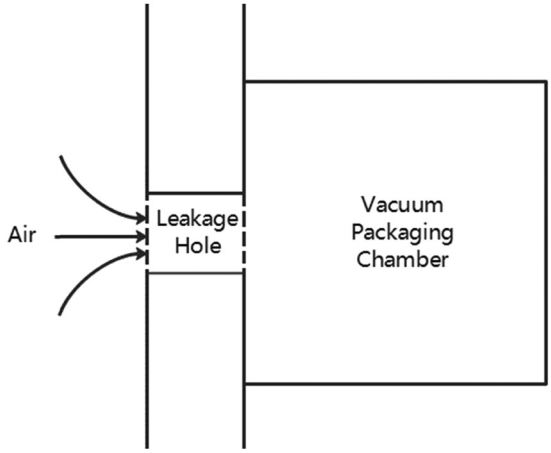

Figure 3: Schematic of vacuum packaging leakage model. This schematic is intended to illustrate the path of the gas into the vacuum packaging chamber, *i.e.*, through the leakage hole into the packaging chamber.

where d and L represent the diameter and length of the capillary tube, respectively, η (Pa s) is the viscosity coefficient of the gas, M (kg/mol) represents the relative molecular weight of the gas, T (K) represents the absolute temperature of the gas, R is the ideal gas constant, which is 8.31 Pa m^3 mol^{-1} K^{-1}, p_1 and p_2 are the pressures at the inlet and outlet of the channels, and $\bar{p}$ represents the average pressure in the tube.

The ideal gas law equation is shown below:

$$pV = nRT \tag{2}$$

And the density per unit pressure ρ is introduced, which can be expressed by:

$$\rho = \frac{m}{pV} = \frac{nM}{pV} = \frac{nM}{nRT} = \frac{M}{RT} \tag{3}$$

According to the equation above, formula (1) could be simplified as

$$Q = \frac{\pi d^4 \bar{p}}{128\eta L}(p_1 - p_2) + \frac{1}{6} b \left(\frac{2\pi}{\rho}\right)^{1/2} \frac{d^3}{L}(p_1 - p_2) \tag{4}$$

$$b = \frac{1 + \frac{\sqrt{\rho}}{\eta} d\bar{p}}{1 + 1.24\frac{\sqrt{\rho}}{\eta} d\bar{p}} \tag{5}$$

As can be seen from (4) and (5), the gas leakage is related to the capillary structural parameters and the difference between internal and external pressures. The gas leakage rate is proportional to the third or fourth square of the capillary channel diameter, d, and inversely proportional to the capillary hole length L. Leakage rate can be reduced by decreasing the diameter or increasing the length of the capillary tube. The gas leakage rate is also proportional to the pressure difference at both sides of the channels. Gas leakage stops when the pressure difference between the two sides of the channel is zero.

The above gas leakage is derived according to Newton's law. When the quality of vacuum welding is poor, it is obvious that the outside air will quickly leak into the metal shell. With the improvement in welding quality, the diameter of the leakage hole will be further reduced.

In this study, a tuning fork crystal oscillator is used to measure the change in air pressure inside the vacuum cavity of a metal channel shell as the welding quality improves. The MD2A shell was vacuum packaged in 2005 with a crystal oscillator inside the vacuum packaging to measure the vacuum. The resonant impedance of the crystal oscillator varies greatly with air pressure when the X- and Y-cut quartz oscillator is operating in bending oscillation mode. The direct digital frequency synthesizer (DDS) module is used to output a sinusoidal signal of analog scanning frequency, phase, and amplitude. The sinusoidal signal is filtered by a low-pass filter (LPF) unit and the final waveform is output to excite the crystal circuit at the end. As the crystal oscillator is connected to a resistor network, when the crystal reaches resonance, *i.e.*, the crystal oscillator behaves as a pure impedance.

$$Z = R + \mathrm{j}\omega L - j\frac{1}{\omega C} = R \tag{6}$$

The resistance of the crystal oscillator at resonance is obtained by comparing the two voltage values at the front and end of the crystal oscillator. In this measurement system, the output is the voltage value.

In this study, the metal tube shell with the crystal oscillator inside is vacuum welded using resistance welding equipment in a vacuum environment. The leakage rate of the vacuum packaged tube shell is about 10^{-8} to 10^{-9} Pa m^3/s. This leakage rate indicates that there are nanotubes in the metal tube shell after packaging, if there are no nanotubes, the leakage rate should be about 10^{-11} to 10^{-12} Pa m^3/s. According to the previous theoretical calculation, it is expected that the vacuum packaged tube shell will leak fast. However, after 12 years of test and observation, the vacuum inside the vacuum packaged channels shell is maintained as shown in Figure 4; it is found that the channels shell has been kept in vacuum for 12 years. Although there are fluctuations, no significant reduction in a vacuum was observed. The 12 years of vacuum packaging measurements show that when the diameter of the nanochannels is reduced to a certain degree, although there is a pressure difference of 1 atmosphere at both ends of the channels, there is a hindrance to the gas flow in the channels.

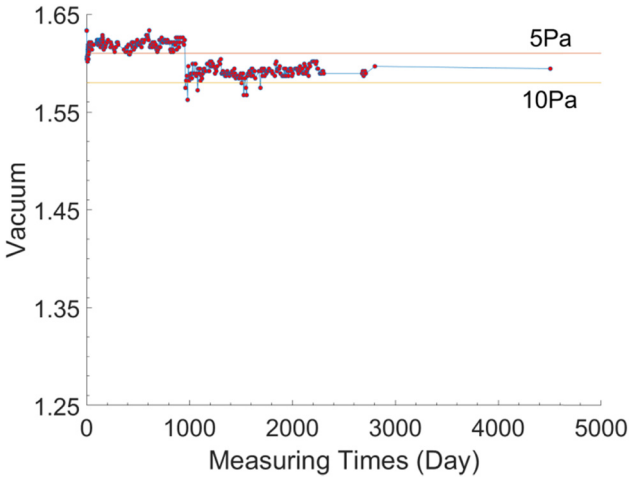

Figure 4: Relationship between vacuum holding voltage and time in vacuum packaging shell. According to the experimental data, the vacuum level kept fluctuating in a stable range until day 954 while there was a significant decrease from the 954th day to the 961st day, and continued to fluctuate in a stable range after the 961st day, until the 5,355th day, when the vacuum level remained at 1.5512. Data on the vacuum holding time of other packing shells are shown in the Appendix.

Thus, the theoretical calculations are quite different from the experimental results, which further shows that the mechanism of airflow in the macroscopic channels will no longer apply to the nanochannels.

3 Discussion

When the leakage holes of metal tube shells are small and reach the nanometer level, this study introduces the De Broglie's Matter Waves and Heisenberg's uncertainty principle in quantum mechanics to analyze the air molecular flow.

Similar to the diffraction that occurs when a particle passes through a single slit, as shown in Figure 5, this study assumes that air molecules will also diffract when passing through nanochannels. The phenomenon exhibits that they are a form of waves, as shown in Figure 6, based on De Broglie's Matter Waves. These molecules will have momentum perpendicular to their original direction of motion when diffraction occurs, and the momentum in this perpendicular direction has uncertainty.

According to Heisenberg's uncertainty principle, the more accurately we know the position of an air molecule, the less accurately we know its momentum. Then the less accurately we know the momentum in the vertical

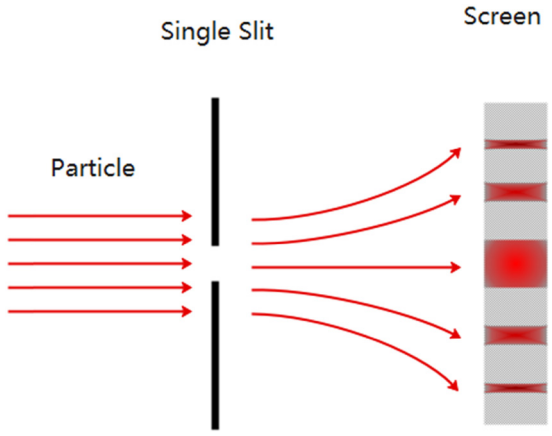

Figure 5: Single-slit diffraction pattern of particles. In the process of light propagation, when it encounters an obstacle or a small hole, the light will deviate from the straight path of propagation and travel around behind the obstacle. This study assumes that air molecules will also diffract when passing through nanochannels.

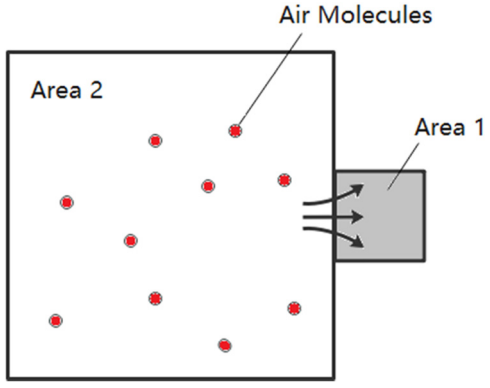

Figure 6: Section of nanochannels. This diagram demonstrates that air molecules also pass through tiny tubes as they move from area 2 to area 1.

direction and the greater the resistance to the original direction of motion of molecules after collision with the wall of the channel. While it is not possible to exactly know the motion of individual molecules, it is possible to know the statistical pattern of the motion of many molecules. Since the mean free path of air molecules ($\bar{\lambda} = 6.805 \times 10^{-8}$ m) is greater than the diameter of the nanochannels, most of the collisions in the vertical direction are particle-to-channels wall collisions, and the horizontal direction collisions are particle-to-particle collisions, as shown in Figure 7. The probability of particle collisions in the vertical direction is much larger than that of collisions in the horizontal direction.

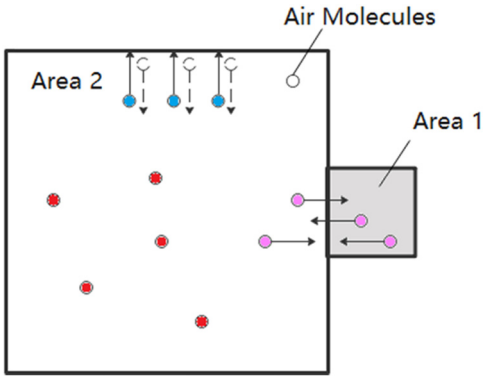

Figure 7: Schematic diagram of air molecular collision in the channels. This diagram demonstrates the possible movements of air molecules from area 2 to area 1, one is to stop at area 2, the other is to pass through a small pipe to area 1, and some will collide with the sidewalls of area 2.

According to Heisenberg's uncertainty principle

$$\Delta x \Delta p \geq \frac{h}{4\pi}, \tag{7}$$

where Δx represents the uncertainty of position and Δp represents the uncertainty of the momentum.

The nanochannels model of the metal shell can be simplified as shown in Figure 5, in which area 1 of the channels is connected to area 2, and both are simplified to cube structures. Air is filled inside the channels, and air molecules can be set as microscopic particles in quantum mechanics. The above nanochannels model is packaged in a vacuum environment of 10 Pa.

In area 1, we have the equation (8):

$$\Delta x_1 \Delta p_1 \geq \frac{h}{4\pi}, \tag{8}$$

where Δx_1 represents the uncertainty of the position of the air molecules in area 1, and Δp_1 represents the uncertainty of the momentum of these molecules.

It can be deduced from equation (8) that

$$\Delta p_1 \geq \frac{h}{4\pi \Delta x_1} = A \tag{9}$$

In area 2, we have equation (10):

$$\Delta x_2 \Delta p_2 \geq \frac{h}{4\pi}, \tag{10}$$

where Δx_2 represents the uncertainty of the position of the air molecules in area 2, and Δp_2 represents the uncertainty of the momentum of these molecules.

It can be deduced from equation (10) that

$$\Delta p_2 \geq \frac{h}{4\pi \Delta x_2} = B \tag{11}$$

Since the volume of area 2 is larger than that of area 1, we can get the expression: $\Delta x_2 > \Delta x_1$, which also means $A > B$. Then we can obtain $\Delta p_1 > \Delta p_2$. It means that the uncertainty of the momentum of air molecules in area 1 is larger than the uncertainty of the momentum of air molecules in area 2. As areas 1 and 2 are connected, the air molecules inside can flow with each other, then the momentum uncertainty of areas 1 and 2 will change. If some air molecules flow from area 2 to area 1, the uncertainty in the momentum of these molecules will be counted with the original molecules in area 1, and the uncertainty in the momentum of the molecules in area 1 will be reduced with high probability. As the flow continues, the momentum uncertainty of the existing molecules in area 1 will continue to get smaller until it reaches A – the minimum value of the momentum uncertainty of the molecules in area 1. At this time, there will no longer be a batch of air molecules flowing from area 2 to area 1. If any, the momentum uncertainty quantity of molecules in area 1 will be further reduced, making it lower than A, which is contrary to Heisenberg's uncertainty principle.

The gap between the molecules of gas under vacuum at room temperature is very large, and the molecular spacing reaches more than 10 times the order of magnitude of the molecular diameter, and the interaction force between the molecules is very weak and can be ignored. In addition to the collision of gas molecules with each other and the collision with the wall of the leaky hole, it is regarded as a completely elastic collision. The pressure on the wall at the collision can be calculated by using the momentum theorem, then we can obtain:

$$P = \frac{nmv^2}{3V}, \tag{12}$$

where n is the total number of leakage gas molecules, v is the rate, and V is the volume of the leakage hole.

Consider the average kinetic energy of the gas molecules,

$$E_k = \frac{mv^2}{2} \tag{13}$$

Since the average kinetic energy of the gas molecules is proportional to the thermodynamic temperature,

$$E_k = \frac{3}{2}KT \tag{14}$$

It can be seen from equation (14) that the energy is discontinuous and the temperature is also discontinuous.

By combining equations (12–14), pressure can be described as follows

$$P = \frac{nmv^2}{3V} = \frac{2nE_k}{3V} = \frac{nKT}{V}, \tag{15}$$

where K is Boltzmann's constant and T is the thermodynamic temperature. From formula (15), it can be seen that the pressure is also discontinuous when n and V are constant.

Think about the 1-D case:

$$\Delta x \Delta \sqrt{\frac{3mPV}{n}} \geq \frac{h}{4\pi} \tag{16}$$

$$\Delta \sqrt{\frac{3mPV}{n}} \geq \frac{h}{4\pi} / \Delta x \tag{17}$$

Since the ratio of n to V is constant when packaged in a vacuum chamber, then we can obtain

$$\sqrt{\frac{3mV}{n}} \Delta(\sqrt{P}) \geq \frac{h}{4\pi} / \Delta x \tag{18}$$

According to Heisenberg's uncertainty principle, when the uncertainty of position becomes smaller, the uncertainty of momentum will increase, and the uncertainty of $\sqrt{P}$ will increase when momentum is represented by pressure P. The uncertainty of pressure P will increase, and the mean value of pressure P will increase, making the gas at that location be the local high pressure, thus blocking the passage of the gas flow. The 12-year vacuum packaging experiments have shown that when the diameter of the nanochannels is reduced to a certain level, there is a hindrance to the gas flow in the channels despite a pressure difference of 1 atm between the two ends of the channels. According to the previous analysis, the hindrance is caused by the local high pressure. The local high pressure in area 1 is caused by the quantum effect of gas in the nanochannels of area 1. The local high pressure in area 1 will not drive the gas flow into area 2 of the channels and the pressure is quantized. This localized high pressure is the result of the accumulation of air molecules in a small space, which interact with the atoms of the channel wall to form adhesions. Even if adhesion occurs, the air molecules are not stationary.

4 Conclusion

This article introduces quantum mechanics into nanochannels gas fluid dynamics for the first time, expanding the new direction of fluid mechanics.

(1) Twelve years of vacuum packaging experiments show that when the diameter of the nanochannels are reduced to a certain level, there is a hindrance to the gas flow in the channels even though there is a pressure difference of 1 atmosphere between the two ends of the channels.
(2) When the diameter of the nanochannels is reduced to a certain degree, the gas flow in the channels is fluctuating.
(3) When the diameter of the nanochannels is reduced to a certain degree, the gas is locally at high pressure at the minimum diameter.
(4) Leakage rate detection values indicate the presence of nanochannels after the packaging of the metal shell.

Funding information: The authors state no funding involved.

Author contributions: All authors have accepted responsibility for the entire content of this manuscript and approved its submission.

Conflict of interest: The authors state no conflict of interest.

Data availability statement: The datasets generated during and/or analysed during the current study are available from the corresponding author on reasonable request.

References

[1] Knudsen M. Die Gesetze der Molekularstromung und der inneren riebungsstromung der gase durch rohnen. Ann Phys. 1909;333(5):999–16.
[2] Scorrano G, Bruno G, Trani DN, Ferrari M, Pimpinelli A, Grattoni A. Gas flow at the ultra-nanoscale: universal predictive model and validation in nanochannels of Ångstrom-level resolution. ACS Appl Mater Interfaces. 2018;10(38):32233–8.
[3] Sartipzadeh O, Naghib SM, Shokati F, Rahmanian M, Majidzadeh-A K, Zare Y, et al. Microfluidic-assisted synthesis and modelling of monodispersed magnetic nanocomposites for biomedical applications. Nanotechnol Rev. 2020;9(1):1397–1407.
[4] Wu T, Zhang D. Impact of adsorption on gas transport in nanopores. Sci Rep. 2016;6:23629.
[5] Ding L, Wei Y, Li L, Zhang T, Wang H, Xue J, et al. MXene molecular sieving membranes for highly efficient gas separation. Nat Commun. 2018;9(1):155.
[6] Park HB, Kamcev J, Robeson LM, Elimelech M, Freeman BD. Maximizing the right stuff: The trade-off between membrane permeability and selectivity. Science. 2017;356(6343):eaab0530.
[7] Chang N, Gu ZY, Wang HF, Yan XP. Metal–organic-framework-based tandem molecular sieves as a dual platform for selective

microextraction and high-resolution gas chromatographic separation of N-alkanes in complex matrixes. Anal Chem. 2011;83:7094–101.
[8] Zhang J, Pei G, Zhang L. Molecular dynamics simulation of methane gas flow in nanopores. Petroleum. 2019;5(3):252–9.
[9] Wang Z, Cai K, Lu Y, Wu H, Li Y, Zhou Q. Insight into the working wavelength of hotspot effects generated by popular nanostructures. Nanotechnol Rev. 2019;8(1):24–34.
[10] Wang R, Peng F, Song K, Feng G, Guo Z. Molecular dynamics study of interfacial properties in CO_2, enhanced oil recovery. Fluid Phase Equil. 2018;467(15):25–32.
[11] Jin Z, Firoozabadi A. Flow of methane in shale nanopores at low and high pressure by molecular dynamics simulations. J Chem Phys. 2015;143(10):104315.
[12] Song X, Chen JK. A comparative study on poiseuille flow of simple fluids through cylindrical and slit-like nanochannels. Int J Heat Mass Tran. 2018;51(7):1770–9.
[13] Liu Y, Wilcox J. Molecular simulation of CO_2 adsorption in micro- and meso-porous carbons with surface heterogeneity. Int J Coal Geol. 2012;104(1):83–95.
[14] Baek S, Akkutlu IY. Mean free path of gas molecules in organic nanochannels using molecular simulations. SPE J. 2019;24(6):2555–73.
[15] Ma W, Jiang Y, Zhang H, Zhang L, Hu J, Jiang L. Miniature on-fiber extrinsic fabry-perot interferometric vibration sensors based on micro-cantilever beam. Nanotechnol Rev. 2019;8(1):293–8.
[16] Arlemark EJ, Reese JM. Investigating the effect of solid boundaries on the gas molecular mean-free-path. Proceedings of the ASME 2009 7th international conference on nanochannels, microchannels, and minichannels, Pohang, South Korea; 2009 June 22–24. p. 397–405.
[17] Arlemark EJ, Dadzie SK, Reese JM. An extension to the Navier-Stokes equations to incorporate gas molecular collisions with boundaries. J Heat Transfer. 2010;132(4):041006.
[18] Fichman M, Hetsroni G. Viscosity and slip velocity in gas flow in microchannels. Phys Fluids. 2005;17(12):123102.
[19] Javadpour F, Fisher D, Unsworth M. Nanoscale gas flow in shale gas sediments. J Can Pet Technol. 2007;46(10):55–61.
[20] Hong C, Shigeishi T, Asako Y, Faghri M. Experimental investigations of local friction factors of laminar and turbulent gas flows in smooth micro-tubes. Int J Heat Mass Transfer. 2020;158:120035.
[21] Ma W, Jiang Y, Zhang H, Zhang L, Hu J, Jiang L. Miniature on-fiber extrinsic fabry-perot interferometric vibration sensors based on micro-cantilever beam. Nanotechnol Rev. 2019;8(1):293–8.
[22] Choi SB, Barron RF, Warrington RO. Fluid flow and heat transfer in microtubes. Micromech Sens Actuat Syst. 1991;32:123–34.
[23] Celata GP, Lorenzini M, Morini GL, Zummo G. Friction factor in micropipe gas flow under laminar, transition and turbulent flow regime. Int J Heat Fluid Flow. 2009;30(5):814–22.
[24] Lorenzini M, Morini GL, Salvigni S. Laminar, transitional and turbulent fric- tion factors for gas flows in smooth and rough microtubes. Int J Therm Sci. 2010;49(2):248–55.
[25] Roohi E, Darbandi M, Mirjalili V. DSMC solution of supersonic to choked sub- sonic flow in micro to nano channels. Proceedings of the ASME 6th international conference on nanochannels, microchannels and minichannels, Darmstadt, Germany; 2008 June 23–25. p. 985–93.
[26] Kermani EL, Roohi E, Porté-Agel F. Evaluating the modulated gradient model in large eddy simulation of channel flow with OpenFOAM. J Turbul. 2018;19(7):600–20.
[27] Arndt M, Nairz O, Vos-Andreae J, Keller C, van der Zouw G, Zeilinger A. Wave–particle duality of C60 molecules. Nature. 1999;401:680–2.
[28] Wang X, Xu P, Han R, Ren J, Li L, Han N, et al. A review on the mechanical properties for thin film and block structure characterised by using nanoscratch test. Nanotechnol Rev. 2019;8(1):628–44.
[29] Zurek WH. Decoherence and the transition from quantum to classical. Phys Today. 1991;1:36–44.
[30] Joos E, Zeh HD, Kiefer C, Giulini DJ, Kupsch J. Decoherence and the appearance of the classical world in quantum theory. Berlin: Springer; 1996.
[31] Grisenti RE, Schöllkopf W, Toennies JP, Manson JR, Savas TA, Smith HI. He atom diffraction from nanostructure transmission gratings: the role of imperfections. Phys Rev A. 2000;61(3):033608.
[32] Chapman MS, Hammond TD, Lenef A, Schmiedmayer J, Rubenstein RA, Smith E, et al. Photon scattering from atoms in an atom interferometer: coherence lost and regained. Phys Rev Lett. 1995;75(21):3783–7.
[33] Werner SA, Colella R, Overhauser AW, Eagen CF. Observation of the phase shift of a neutron due to precession in a magnetic field. Phys Rev Lett. 1975;35:1053–5.
[34] Shayeghi A, Rieser P, Richter G, Sezer U, Rodewald JH, Geyer P, et al. Matter-wave interference of a native polypeptide. Nat Commun. 2020;11:1447.
[35] Simionescu OG, Pachiu C, Ionescu O, Dumbrăvescu N, Buiu O, Popa RC, et al. Nanocrystalline graphite thin layers for low-strain, high-sensitivity piezoresistive sensing. Rev Adv Mater Sci. 2020;59(1):306–13.
[36] Kovachy T, Asenbaum P, Overstreet C, Donnelly CA, Dickerson SM, Sugarbaker A, et al. Quantum superposition at the half-metre scale. Nature. 2015;528:530–3.
[37] Schätti J, Rieser P, Sezer U, Richter G, Geyer P, Rondina GG, et al. Pushing the mass limit for intact launch and photoionization of large neutral biopolymers. Commun Chem. 2018;1:93.
[38] Parker RH, Yu C, Zhong W, Estey B, Müller H. Measurement of the fine-structure constant as a test of the standard model. Science. 2018;360(6385):191–5.
[39] Rodewald J, Dörre N, Grimaldi A, Geyer P, Felix L, Mayor M, et al. Isotope-selective high-order interferometry with large organic molecules in free fall. New J Phys. 2018;20:033016.
[40] Nimmrichter S, Hornberger K, Haslinger P, Arndt M. Testing spontaneous localization theories with matter-wave interferometry. Phys Rev A. 2011;83(4):043621.
[41] Zeng J. Quantum mechanics. 5th ed. Beijing: Science Press; 2019.
[42] Jahangir A, Malik F, Muhammad N, Fayyaz R, Abbasi JN, Nazir A. Reflection phenomena of waves through rotating elastic medium with micro-temperature effect. Rev Adv Mater Sci. 2020;59(1):455–63.
[43] Basdevant JL, Dalibaed J. The quantum mechanics solver: how to apply quantum theory to modern physics. 3rd ed. Berlin: Springer; 2005.
[44] Landau LD, Lifshiz EM. Quantum mechanics, non-relativistic theory. 3rd ed. Oxford: Pergamon Press; 1977.

[45] Merzbacher E. Quantum mechanics. 3rd ed. New York: Wiley; 1970.
[46] Robinett RW. Quantum mechanic: classical results, modern systems, and visualized examples. 2nd ed. New York: Oxford University Press; 2006.
[47] Da D. Vacuum design manual. 3rd ed. Beijing: National Defense Industrial Press; 2004.
[48] Dash CS, Prabaharan SRS. Nano resistive memory (Re-RAM) devices and their applications. Rev Adv Mater Sci. 2019;58(1):248–70.

Appendix

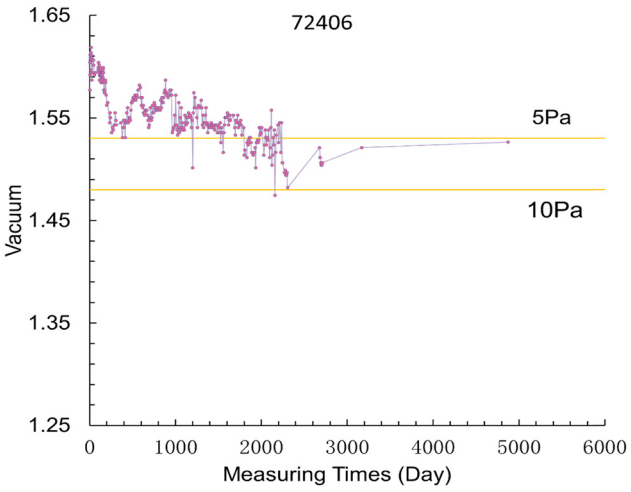

Figure A1: Relationship between vacuum holding voltage and time in No. 72406 vacuum packaging shell.

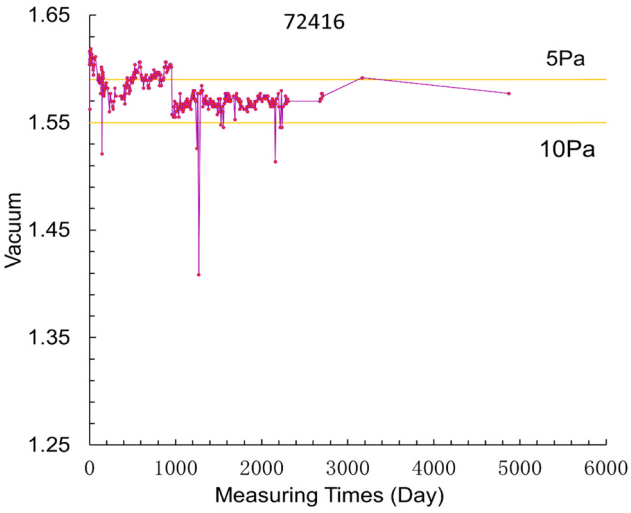

Figure A3: Relationship between vacuum holding voltage and time in No. 72416 vacuum packaging shell.

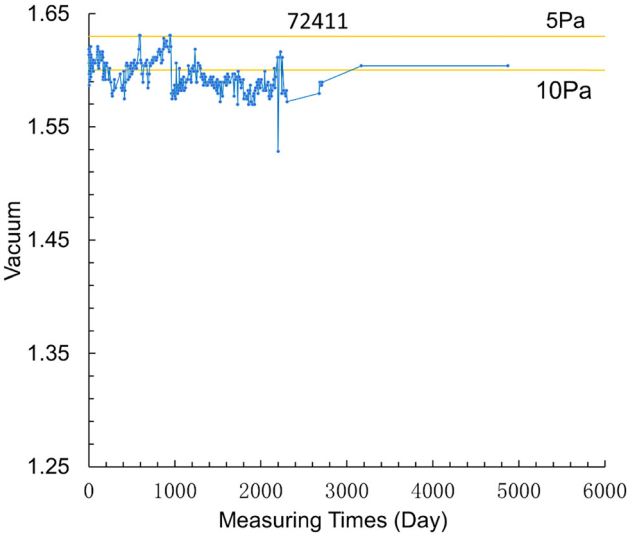

Figure A2: Relationship between vacuum holding voltage and time in No. 72411 vacuum packaging shell.

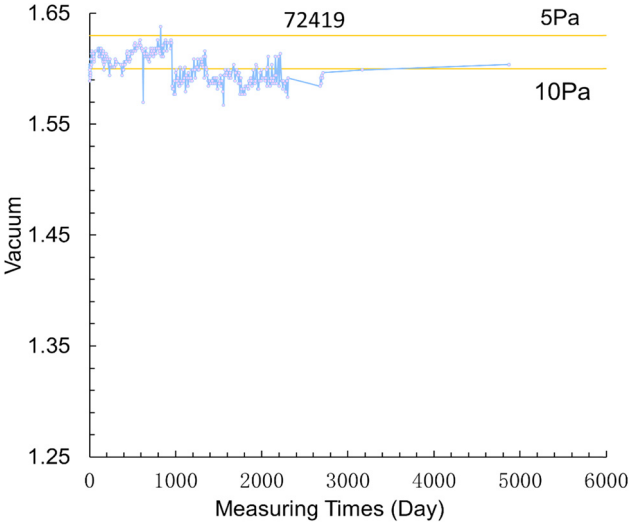

Figure A4: Relationship between vacuum holding voltage and time in No. 72419 vacuum packaging shell.

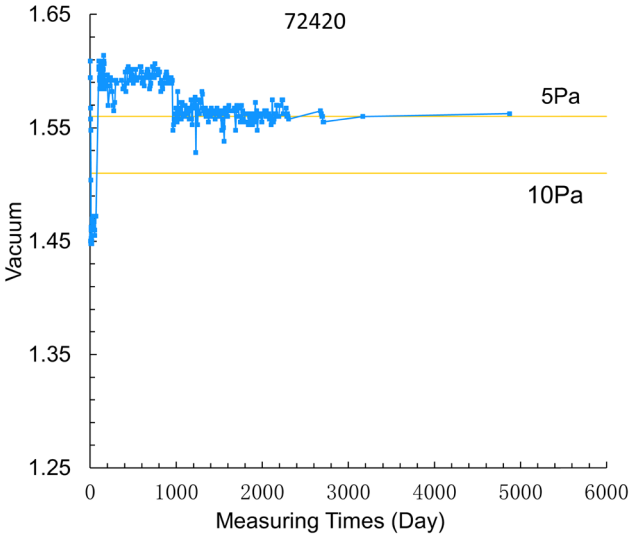

Figure A5: Relationship between vacuum holding voltage and time in No. 72420 vacuum packaging shell.